Improvement of the Temperature Stability of the Erbium-Doped Superfluorescent Fiber Source by Tuning the Reflectivity of the Fiber End

SKALSKÝ, M.; HNIDKA, J.; HAVRÁNEK, Z.

Journal of Lightwave Technology

ISSN: 1558-2213

DOI: https://doi.org/10.1109/JLT.2022.3226206

Accepted manuscript

Improvement of the Temperature Stability of the Erbium-doped Superfluorescent Fiber Source by Tuning the Reflectivity of the Fiber End

Michal Skalský, Jakub Hnidka and Zdeněk Havránek

***Abstract*—A novel and simple way of improving the mean wavelength temperature stability of the erbium-doped superfluorescent source is described and demonstrated. We show that by introducing small reflectivity feedback at the unpumped fiber end in the backward-pump superfluorescent source configuration, we can affect an overall temperature dependency of the mean wavelength of the output spectrum. The reflectivity adjustment can be made by an angled fiber cleave, varying the reflectivity between 0 to 4 %, or by a fusion arc, allowing its finer adjustment. With this approach, we were able to arbitrarily adjust the mean wavelength temperature trend from -4.38 to 5.23 ppm/°C. Furthermore, an optimal reflectivity was attained, providing almost zero trend and reducing the total mean wavelength variation to 130 ppm over the temperature range of -40 to +100 °C, which is a 5.7-fold and 4.4-fold improvement compared to 0° and a standard 8° fiber cleave angle, respectively. By avoiding any filtering components, a wide bandwidth of 37.8 nm and a power efficiency of 22% was reached. Since the proposed configuration does not include any extra components compared to the basic backward-pump configuration, it can be a viable solution for cost-efficient applications, such as, e.g., medium-grade fiber-optic gyroscopes. A benefit for these gyroscopes is the tunability of the source wavelength temperature dependency which can conveniently compensate the gyro coil temperature sensitivity.**

***Index Terms*—Er-doped superfluorescent source, fiber-optic gyroscope, temperature stability, cleave angle, reflectivity, double-pass.**

I. Introduction

The superfluorescent fiber sources (SFS) with an Erbuim-doped (Er-doped) fiber are used together with superluminescent diodes (SLD) as a source in fiber-optic gyroscopes (FOG) due to their broadband spectrum [1]–[3] to suppress parasitic effects such as Kerr, Shupe, or Rayleigh backreflection [4]. Compared to SLDs, the current SFSs exhibit by about two to three orders better thermal stability, which is crucial for the high-grade FOGs. Moreover, they can provide a high power conversion efficiency [5], [6] even with limited pump power and COTS components, and thus represent a viable solution in terms of price-to-power ratio.

In a relation to FOGs, typical studied issues of the SFS include maximizing a spectrum width [7]–[9] and flatness [6], [7], [10], [11], minimizing a radiation sensitivity [12], [13], but majority of the studies are dedicated to minimizing a temperature sensitivity [3], [14]–[24]. As the measured angular velocity by the FOG is proportional to the Sagnac phase shift with a scale factor depending on the used wavelength, the SFS mean wavelength stability is the most critical parameter. Optical output signal is also proportional to the SFS power, but this dependency can be suppressed by an inherent insensitivity for a closed-loop operation [1], [25], or by specific compensation techniques in case of open-loop FOGs [26], [27].

So far, many approaches have been proposed to enhance the SFS mean wavelength temperature stability, such as long period grating [15], fiber Bragg grating [16], [28], photonic bandgap filter [17], thin film filter [11], [29], Er-doped fiber filter [8], [14], [22], [23], also photonic crystal Er-doped fiber [18], Faraday rotator mirror [19], [20], [30], or variable parameters control [24].

Although these solutions are able to provide excellent temperature stability, reaching 1 ppm/°C or better, we need to consider their limitations as well.

Firstly, most of the nowadays techniques are based on filtering, commonly near dominant spectrum peaks around 1530 or 1560 nm [21]. This yields two considerable consequences. One is a limited spectral width, which has a negative impact on the minimal detectable angular rate of the FOG due to the noise increase [31]. The other is decreased power efficiency, i.e., to achieve the same output power we need to employ higher pump power, or a longer fiber, both of which mean increase in the final price or energy consumption. In cost and power sensitive applications, e.g., automotive, these parameters may be especially crucial. Secondly, such techniques mostly employ additional optical components in the SFS, often custom-made and with a proprietary design, which further increases the total SFS complexity and cost. In the navigation grade FOGs, where SFS stability should not exceed 1 ppm [31],

The work has been performed in the project NewControl: Integrated, Fail-Operational, Cognitive Perception, Planning and Control Systems for Highly Automated Vehicles, under grant agreement No. 826653/8A19006. The work was co-funded by grants of Ministry of Education, Youth and Sports of the Czech Republic and Electronic Component Systems for European Leadership Joint Undertaking (ECSEL JU). The work was supported by the infrastructure of RICAIP that has received funding from the European Union's Horizon 2020 research and innovation programme under grant agreement No. 857306 and from Ministry of Education, Youth and Sports under OP RDE grant agreement No. CZ.02.1.01/0.0/0.0/17043/0010085. The completion of this paper was also made possible by the grant No. FEKT-S-20-6205 "Research in Automation, Cybernetics and Artificial Intelligence within Industry 4.0" financially supported by the Internal science fund of Brno University of Technology.

The authors are with the Central European Institute of Technology, Brno University of Technology, Brno, Czech Republic (e-mail: michal.skalsky@ceitec.vutbr.cz; jakub.hnidka@ceitec.vutbr.cz; zdenek.havranek@ceitec.vutbr.cz).

this usually does not pose a problem. Nevertheless, the lower-grade FOGs, which can also benefit from SFS advantages, have more strict requirements on the cost-efficiency, therefore, simpler solutions are generally preferable [32].

A very simple method for the mean wavelength stabilization of the double pass backward-pumped (DPB) SFS was presented in [33], where the temperature sensitivity was decreased by replacing a mirror at the free Er-doped fiber end by a perpendicular fiber cleaving providing a 0.04% reflection, showing the change of the backreflected power can have an impact to the SFS mean wavelength temperature stability. Therefore, an assumption can be made that by a meaningful manipulation of the reflected power, it could be possible to optimize the mean wavelength temperature dependency of the SFS. While the perpendicular cleave may be the optimal solution only in case of specific conditions (fiber length, Er concentration and profile, the pump power and wavelength, etc.), an arbitrary handling of the backreflected power might be a useful mechanism to optimize the SFS temperature behavior in general case. It is important to note that a zero temperature sensitivity of the SFS is not always required. In many cases it is more convenient to compensate the inherent FOG temperature dependency caused by the fiber expansion by an opposite sensitivity of the SFS to improve an overall temperature stability of the FOG scale factor [34].

In this paper, we provide a simple and inexpensive method of adjusting the backward-pumped SFS mean wavelength temperature coefficient through the adjustment of the reflectivity of the unpumped Er fiber end by a tilted cleave with an optional thermal fine-tuning. Since it is based on a reflection at the unpumped end, where the feedback is considerably weak, it can be called a weak-feedback double-pass (WF-DPB) SFS.

The sole equipment required is a fiber cleaver with an angle cleaving, a fiber splicer and an optical spectrum analyzer (OSA). With this setup, it was possible to attain a stability of 130 ppm over the temperature range from -40 to 100 °C and ∼22% pump conversion efficiency with a basic DPB architecture only. To our knowledge, this is the simplest method of the mean wavelength temperature stabilization reported so far, providing an acceptable level of stability. Concurrently, it exceeds the filtering-based methods in its bandwidth and power efficiency.

II. Principles

The erbium ions inside the silica optical fiber enable it to behave as an active medium capable of absorbing and emitting energy in the form of photons [35], [36]. The Er-doped fiber is usually described by the three-level energy diagram explaining possible transitions, which can be either radiative, or nonradiative [37], [38]. Due to Stark split of each energy level, the Er-doped fibers can absorb and emit various quanta of energy. This is usually characterized by its absorption and the emission spectra cross sections [5], [38]. The spectra cross sections of the fiber used in the experiments are shown in Fig. 1 [39]. We can see a partial overlap between the spectra, meaning the Er ions are capable

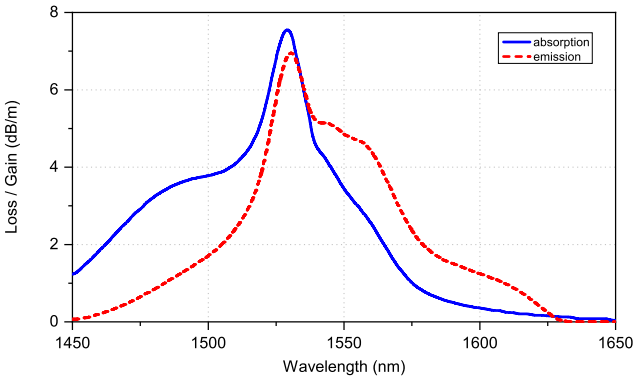

Fig. 1. Absorption and emission spectrum cross section of the used fiber (Fibercore I-6(980/125)).

of absorbing and emitting light at similar wavelengths. The absorption spectrum is slightly shifted towards the shorter wavelengths compared to the emission spectrum, resulting in some energy loss in Er ions, which can be explained by the presence of the nonradiative transitions. Comparing the emission and the absorption spectra, we can deduce the most efficient wavelengths for the pump (i.e., yielding the highest reachable gain), which are 980 (out of scale in Fig. 1) and 1480 nm [38]. Generally, the shape of the output broadband SFS spectrum can vary, depending on the SFS configuration, the pump power and the wavelength, Er fiber type and its length, and parameters of the additional components, such as reflectors, filters, etc. The principle behind the broadband SFS output spectrum is called an amplified spontaneous emission (ASE). This phenomenon generally exists in both forward (pump direction) and backward (opposite direction) directions inside the Er-doped fiber. In the output SFS spectrum, both ASE spectra are combined. Furthermore, when the ASE passes through the highly-pumped region of the Er fiber (i.e., with a high population inversion), it is simply amplified through the gain given by the emission cross section, with a dominant peak around 1530 nm. On the other hand, the lowly-pumped region of the fiber causes filtering of the ASE by the absorption emission cross section, facilitating a rise and even a possible dominance of the 1560 nm peak [12], [36].

Due to the uneven shape of the SFS output spectrum, the characteristic parameters of the FOG, such as the mean wavelength $\overline{\lambda}$ and the spectral width $\Delta\lambda$, cannot be calculated as a peak center or -3 dB drop, respectively. Instead, the following formulas are used [31]:

$$\overline{\lambda} = \frac{\int P(\lambda) \cdot \lambda \, \mathrm{d}\lambda}{\int P(\lambda) \, \mathrm{d}\lambda}, \tag{1}$$

$$\Delta\lambda = \frac{\left[\int P(\lambda) \, \mathrm{d}\lambda\right]^2}{\int \left[P(\lambda)\right]^2 \, \mathrm{d}\lambda}, \tag{2}$$

where the $P(\lambda)$ represents the power spectral density. The

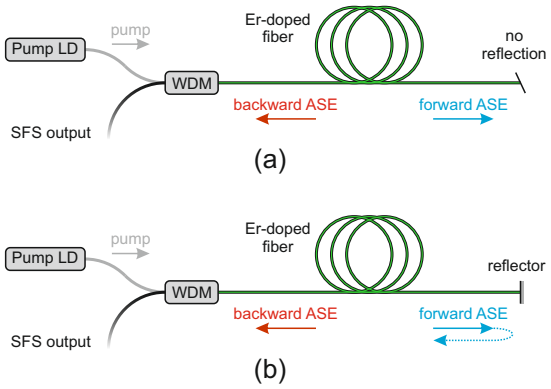

Fig. 2. Basic backward-pump SFS configurations with the ASE power propagation: (a) - single-pass (SPB), (b) – double-pass (DPB).

mean wavelength temperature stability can be expressed as:

$$\frac{\mathrm{d}\overline{\lambda}}{\mathrm{d}T} = \frac{\partial\overline{\lambda}}{\partial T} + \left(\frac{\partial\overline{\lambda}}{\partial P_{\mathrm{pump}}}\right)\left(\frac{\partial P_{\mathrm{pump}}}{\partial T}\right) + \\ + \left(\frac{\partial\overline{\lambda}}{\partial \lambda_{\mathrm{pump}}}\right)\left(\frac{\partial \lambda_{\mathrm{pump}}}{\partial T}\right), \tag{3}$$

where the first term represents the intrinsic Er fiber temperature dependency due to the occupation of the energy levels and the transitions varying with the temperature. It was also shown by [5] that the pump laser diode can be designed in such a way that the addition of the latter two terms is nearly zero. The Er fiber intrinsic fiber temperature dependency $\partial\overline{\lambda}/\partial T$, caused by the temperature dependent Boltzmann distribution of electron energies [40], has the dominant impact on the SFS mean wavelength temperature drift [21], [31]. Therefore, in the experimental part, we focus solely on this component of the overall temperature dependency. However, compared to the spectrum-filtering approaches, where the spectral peak with a higher thermal stability is usually selected, we attempt to form the SFS spectrum as a whole, as it is the mean wavelength which directly affects the FOG scale factor, rather than the spectrum shape.

To fully understand the behavior of the SFS central wavelength with temperature, we need to consider how the SFS spectrum can evolve with the temperature in the case of the backward-pump configuration, which is mostly adopted as an SFS source in FOGs [5], [9], [41]. The absorption and emission cross sections were demonstrated to shift towards longer wavelengths with an increase in temperature [21], [38], [42]. The dominant radiative transitions causing emission around 1530 and 1560 nm shift correspondingly [5], [31]. In the case of a simple SPB configuration (Fig. 2a), it might be thus challenging to reach a thermal invariancy of the mean wavelength. To stabilize the mean wavelength, it is either necessary to insert additional components, typically with opposite characteristics, or another solution can be used, which is DPB. The DPB (Fig. 2b) configurations reported nearly flat [14], [20], [22] or even negative temperature dependency of the mean wavelength [9], [29], [33], [34], which is achieved by a combination of the bare SFS parameters and characteristics of the reflector at the unpumped fiber end. In DPB configuration, the forward ASE is totally or partially reflected and amplified. By adding to the backward ASE, we obtain a spectrum having both 1530 and 1560 nm peaks with different power ratios. Despite the fact that both peaks shift with the temperature in a same manner, it is possible to tune the mean wavelength temperature coefficient $K_{\mathrm{T}} = \Delta\overline{\lambda}/\Delta T$ in positive or negative direction. The first arguably apparent solution lies in achieving the specific selectivity of the reflector or other filtering components, which are, unfortunately usually accompanied by a certain loss of SFS power or spectral width. The second approach lies in searching for a specific balance between the backward ASE and the amplified forward ASE so that they combine in an overall spectrum with a desired temperature dependency. Simulations presented in [5] demonstrated that in one SFS configuration, the intrinsic temperature coefficient can reach both positive and negative (including zero) values, depending on the fiber length, i.e., the amount of backreflected ASE. The general principle facilitating such behavior consists in the temperature dependency of the distribution of the dominant transitions between the excited and the ground energy level manifolds of the Er atoms and also the Boltzmann statistics, as mentioned earlier. Nevertheless, the precise modeling of a temperature dependency of a specific SFS design might be challenging due to the limitations of the McCumber theory accuracy for Er-doped glass, as discussed in [43], [44], contrasting relatively small absolute changes of the spectra. However, as the aforementioned principles impact the evolution of the individual spectral peaks, it is possible to experimentally demonstrate that by its methodical observation, a fairly apparent connection between this transformation and the resulting mean wavelength temperature coefficient K_{T} can be found.

III. Design and Experiment

The experiments were performed with the simple backward-pump configuration, such as in the Fig. 2. The major goals of the proposed SFS design, along the temperature characteristics, were also power and cost-efficiency. Since the 1480 nm pump is comparatively costly, albeit more efficient [22], the 980 nm pump is a better solution for inexpensive SFS designs. We used a compact laser diode (Lumentum T13-7402-050) with a peak power of 50 mW and a central wavelength of 975.6 nm at the room temperature. The diode was driven by a constant current of 100 mA producing a power of 42 mW at the input of the Er-doped fiber. To achieve a high power efficiency [5], [12], we employed 20 meters of weakly-doped fiber I-6 (Fibercore), which absorption and emission spectra are shown in the Fig. 1. The pump is separated from the output ASE by a wavelength division multiplexer (WDM) with a 28 dB separation. To prevent a possible feedback from the FOG, a 37dB isolator is placed at the SFS output.

The experimental setup is schematically shown in the Fig. 3. To measure the $\partial\overline{\lambda}/\partial T$ term independently from the pump contribution to the overall mean wavelength stability, only the Er-doped fiber was placed in the temperature chamber (CTS T-65/50), whereas the pump diode was kept at room temperature stabilized around 23.5 °C. The temperature of the

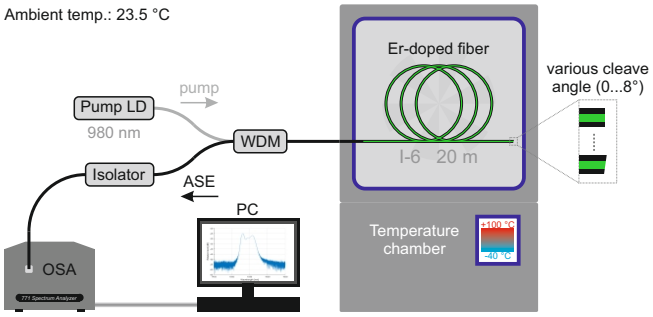

Fig. 3. The experimental setup for SFS output spectra measurement at different temperatures and cleave angles of the Er-doped fiber (LD – laser diode, WDM – wavelength division multiplexer, OSA – optical spectrum analyzer).

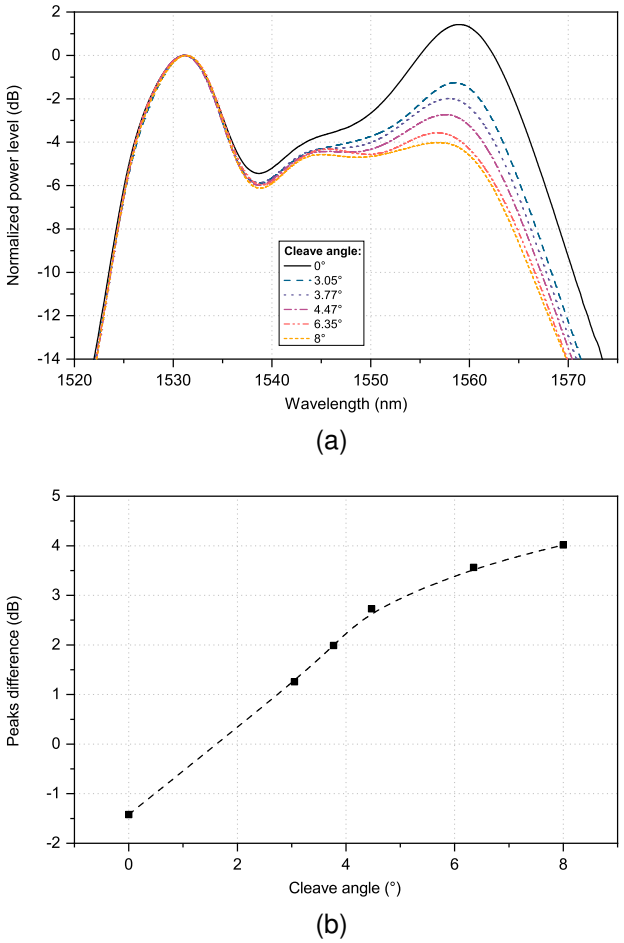

Fig. 4. Comparison of the WF-DPB SFSs with different cleave angles (20 °C): (a) – output spectra normalized to 1530 nm peak, (b) – difference between 1530 and 1560 peaks.

Er-doped fiber was increased from -40 to 100 °C with a fixed step change of 10 °C. At each temperature, a settling time of >10 min was applied before the measurement. The SFS output spectrum was acquired by an optical spectrum analyzer (OSA, Bristol Instruments 771). An attenuator was placed at the input of the OSA to prevent exceeding its power threshold. The unpumped end of the Er-doped fiber was cleaved at different angles by the adjustable angle cleaver (Fujikura CT-101) to adjust the ratio of the reflected power, and thus attain the WF-DPB configuration. The cleave angle was ranging from 0° (perpendicular cleave) to 8°, providing reflections of 3.5% to 0.02%, respectively (at 1550 nm). For a fine tuning of the reflectivity of the fiber tip, we applied a fusion arc using a fusion splicer (Fujikura FSM-100P+) controlled by PC. This procedure enabled to shape the SFS output spectrum with a continuous monitoring through the OSA.

To analyze the SFS behavior with different feedback at the unpumped end, it was necessary to find out the exact cleave angle, as it can be difficult to measure the reflectivity directly due to optical nonlinearity of the Er fiber. Besides 0° and 8° cleave, where the angle was determined based on the cleaver settings, we used a fusion splicer camera to measure the actual cleave angle of other values.

IV. Results and Discussion

Based on the recorded spectra with OSA, the SFS mean wavelength was calculated using the Eq. (1). Due to the residual noise in the spectrum, the calculated central wavelength depends on the wavelength range of the acquired spectrum. Therefore, we performed the calculations for the range of −20 dB down from the peak.

The output spectra of the WF-DPB with different cleave angles are compared in Fig. 4a with a normalization to the power level of the peak around 1530 nm. We can clearly see that as the reflection is decreasing (with increasing angle), the forward ASE, causing a significant peak around 1555–1560 nm, has only a minor impact, and closer to 8° the SFS is purely SPB. This confirms the theoretical assumption, and also the results observed in [33]. We can also see from Fig. 4a that the output spectrum is changing fluently with the angle, which is convenient, since it allows to tune the spectrum shape by the cleaving. The difference between the power levels of the left (around 1530 nm) and the right (around 1560 nm) peak of the spectra shown in the Fig. 4a is plotted in the Fig. 4b, demonstrating the decrease of the right peak level with respect to the left one when the cleave angle is increased.

However, looking at the limit cases with 0 and 8° angle cleave, we can see their behavior with temperature is different. The relative spectra change, obtained as a difference between the spectra measured at different temperatures and the spectrum measured at 20 °C, are shown in the Fig. 5a for 0° cleave and in the Fig. 5b for 8° cleave. In the case of the WF-DPB with a 0° cleave, the rising temperature causes growth of the left peak and simultaneous drop of the right peak, which causes a negative mean wavelength temperature dependency (Fig. 5c). However, in the case of the pure SPB achieved with 8° cleave, we can observe a drop of the left peak. Despite the suppression of the left peak, the power at the longer wavelengths increases, resulting in a positive mean wavelength temperature dependency (Fig. 5d). The dependencies in Fig. 5c,d can be characterized by a slope K_T calculated by a least squares fit, and a standard deviation

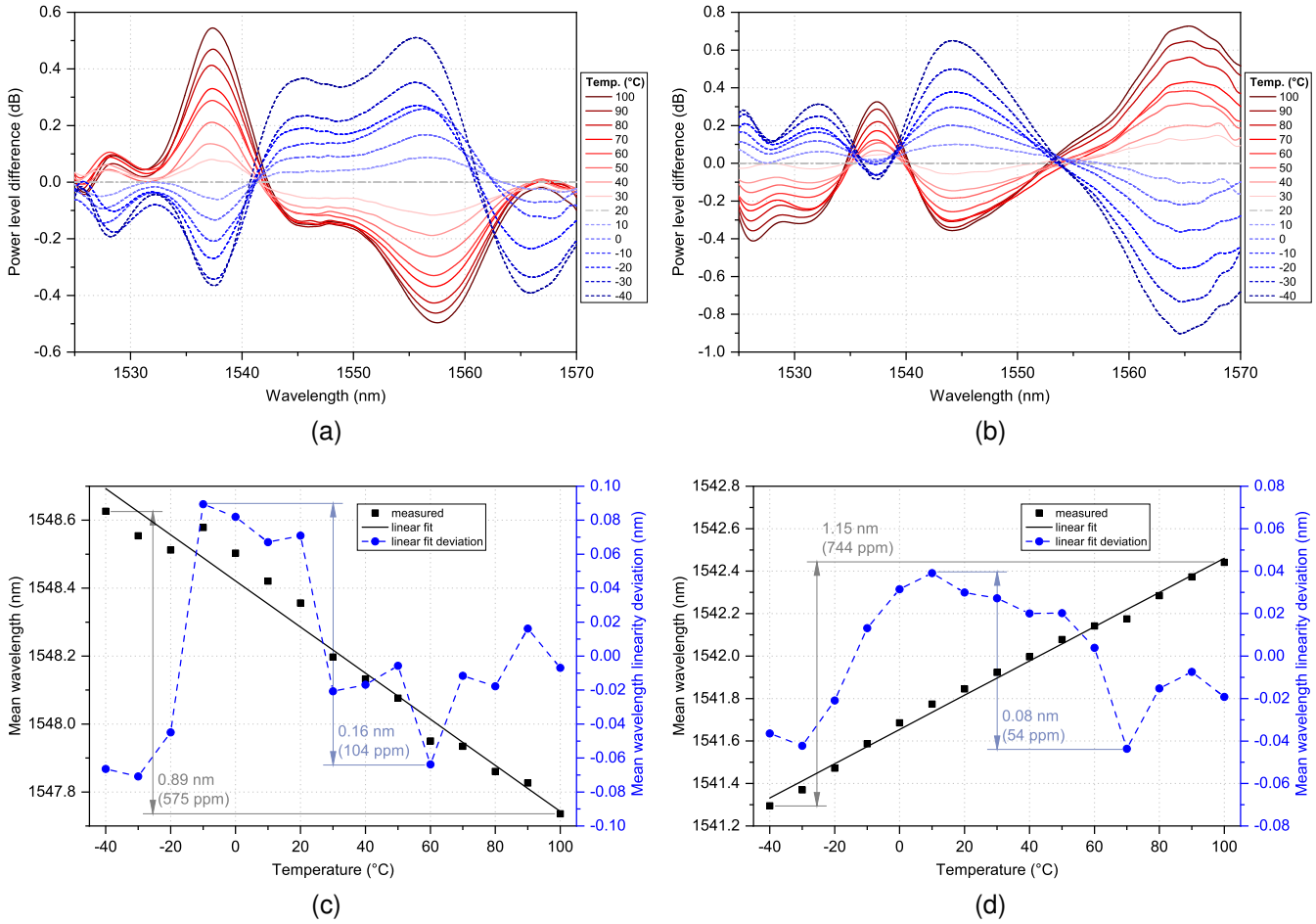

Fig. 5. SFS output spectrum change for 0° and 8° angle cleave: (a) - relative change with respect to the spectrum at 20 °C for 0° cleave, (b) - relative change with respect to the spectrum at 20 °C for 8° cleave, (c) – mean wavelength with temperature for 0° cleave, (d) – mean wavelength with temperature for 8° cleave.

σ_{lin} defined as:

$$\sigma_{\mathrm{lin}} = \sqrt{\frac{1}{N-1}\sum_{i=1}^{N}\left[\overline{\lambda}(T_i) - \overline{\lambda}_{\mathrm{lin}}(T_i)\right]^2}, \qquad (4)$$

where N stands for the number of temperatures, $\overline{\lambda}(T_{\mathrm{i}})$ is the mean wavelength at temperature T_{i}, and $\overline{\lambda}_{\mathrm{lin}}(T) = K_{\mathrm{T}}T + \beta$ is the linear approximation of $\overline{\lambda}(T)$. Whereas the $\overline{\lambda}(T)$ slope has a negative value of $K_{\mathrm{T}} = -6.79$ pm/°C (-4.38 ppm/°C) for 0° cleave, for 8° it reaches a positive value of $K_{\mathrm{T}} = 8.07$ pm/°C (5.23 ppm/°C), suggesting we can actually affect the temperature dependency of a simple WF-DPB only by adding a small amount of feedback facilitating the forward ASE.

The Fig. 6 shows how the slope K_{T} varies with different cleave angles. It can be seen that for this SFS, a temperature invariance of K_{T} can be reached with a cleave angle around 3.6°, corresponding to the reflectivity of 0.37%. However, reaching an angled fiber cleave with a precision better than 0.1° on a majority of commercial cleavers can be an excruciating task. Therefore, we applied a method of cleaving the fiber tip at somewhat larger angle and subsequently tuning the reflectivity of the unpumped end by heating the fiber tip with a fusion splicer. The biggest advantage of this method is that we tune the tip reflectivity in optionally small steps controlled by the adjustment of the arc power. During this process we can also observe the resulting SFS spectrum. In our case, combining the angle dependency of the SFS spectrum peaks difference (Fig. 4b) and the measured temperature dependency

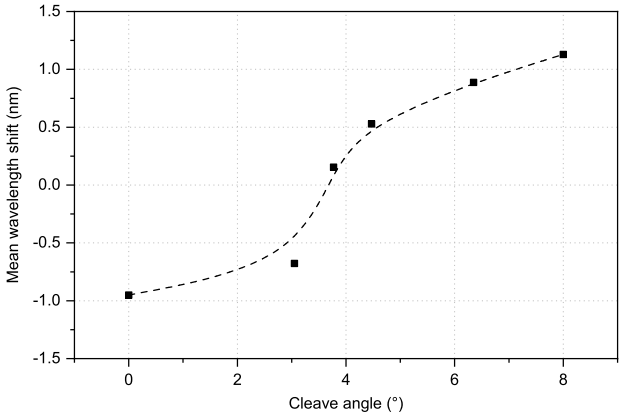

Fig. 6. Dependency of the mean wavelength temperature slope K_{T} on the Er-fiber cleave angle.

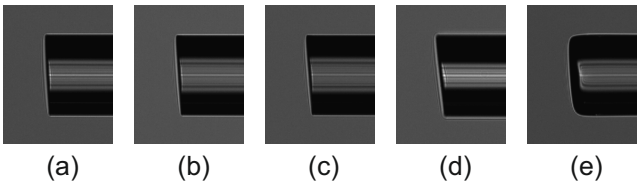

Fig. 7. Er-doped fiber endings with different cleave angles: (a) - 3.05°, (b) - 3.77°, (c) - 4.47°, (d) - 6.35°, (e) – arc modified.

TABLE I
COMPARISON BETWEEN SFSS WITH DIFFERENT FIBER ENDINGS

parameter (unit)	WF-DPB 0° cleave	SPB 8° cleave	WF-DPB arc opt.
Total output power (mW)	10.3	9.2	9.4
Pk-pk $\overline{\lambda}$ variation (nm | ppm)	0.89 | 575	1.15 | 744	0.20 | 130
Spectral width, 20 °C (nm)	37.1	35.0	37.8
Mean wavelength, 20 °C (nm)	1548	1542	1544

of K_{T} (Fig. 6), the optimum peak difference is 1.8 dB at 20 °C.

The fiber endings with different cleave angles used within the experiment are shown in the Fig. 7a-d. For the optimization by the fusion arc method, the identical cleaver settings as for the fiber ending in the Fig. 7b was used. By applying an arc for 0.2 seconds and 400 bit power, we achieved difference of 1.78 dB between the power levels of the two dominant (1530 and 1560 nm) peaks (room temperature of 23.5 °C). The resulting fiber ending is shown in the Fig. 7e. Similarly to the Fig. 5, the output spectrum change due the temperature for the arc-optimized fiber end is shown in the Fig. 8. The changes in the spectrum are comparable to those shown in the Fig. 5a,b in their magnitude. However, in the case of the optimized ending, we can see that the negative power dependency in two ranges around 1530 nm and 1550 nm is in fact compensated by the wavelength regions with an opposite behavior, which are in sum evenly distributed around the mean wavelength of 1544 nm.

The measured mean wavelength temperature drift with respect to the spectrum obtained at 20 °C for all tested reflective endings in the WF-DPB configuration are summarized in the Fig. 9. It can be seen that it is possible to reach an arbitrary slope K_{T} of the mean wavelength temperature dependency solely by adjusting the Er-doped fiber end reflectivity. The standard deviation from the linear fit σ_{lin} was between 19 and 46 ppm over the -40–100 °C temperature range, which satisfies the requirements on the medium-grade FOGs. The comparison of the SFS performance in SPB configuration with an 8° cleave, the WF-DPB configuration with perpendicular cleave, and the WF-DPB configuration with a fiber tip optimized to the reach a minimal intrinsic Er-doped fiber temperature dependency $\partial\overline{\lambda}/\partial T$ is shown in the Table I. Implementing the proposed method, we were able to reach a 5.7-fold and 4.4-fold improvement respectively in terms of a peak-peak variation of the mean wavelength temperature dependency over the investigated temperature range.

Finally, a development of the SFS spectrum shape due to

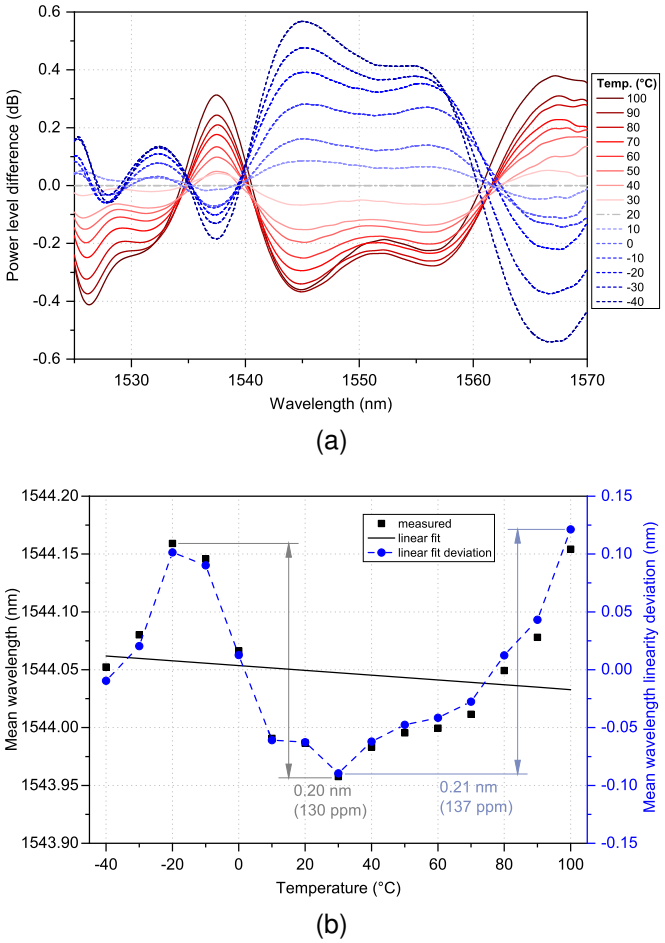

Fig. 8. SFS output spectrum change for arc modified Er-doped fiber ending: (a) - relative change with respect to the spectrum at 20 °C, (b) - mean wavelength with temperature.

temperature change was studied. Due to the Stark split of the erbium energy levels, between which the radiative transitions occur, the SFS spectrum has several peaks, which evolve differently with temperature. To study the separate peaks in the SFS spectrum, we can perform an approximation by a sum of Gaussian functions [38]. In our case, we identified three major peaks with wavelengths around 1531, 1545 and 1558 nm. The examples of the applied spectrum approximation are shown in the Fig. 10 for the SFS configurations from the Table I. By adopting such model, we can observe a shift of both wavelengths as well as power of the individual peaks. The comparison of wavelength and power shifts is shown in the Fig. 11. Based on these characteristics, we can draw general conclusions concerning the SFS emission behavior with temperature. Primarily, we can see that it is necessary to analyze not only the wavelength shifts of the peaks, as is a common approach adopted by the filtering-based methods, but also their power changes. We can observe that the mean wavelength temperature dependency is the largest for the peak around 1558 nm (as seen in the Fig. 11c), confirming the conclusions in [21], and that it is positively correlated with temperature in all studied cases. Nevertheless, the positive wavelength shift with rising temperature is accompanied by the power level decrease of the peak for the arc-optimized

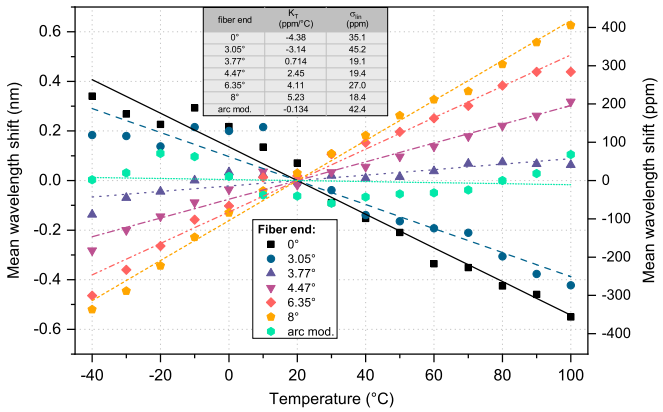

Fig. 9. Comparison of the measured and linearized mean wavelength temperature dependencies normalized to a linearized wavelength at 20 °C for various WF-DPB SFS fiber ends (K_T - mean wavelength temperature dependency slope, σ_{lin} – standard deviation from the linear fit of the mean wavelength).

case (shown in the Fig. 11f), thus its contribution to the overall SFS spectrum, which is a sum of all three peaks, decreases with an increase of the temperature. The overall SFS spectrum is then affected more by the peak around 1531 nm, which power variation is lower (Fig. 11d). In other words, the effects of wavelength and power change are hence balanced in the case of the arc-optimized WF-DPB. Similarly, we could identify additional dependencies of the wavelength and power of the individual spectrum components and, by utilizing the proposed method, it might be possible to further improve the SFS thermal stability optimization. By tuning a single parameter – reflectivity of an unpumped fiber end – it was demonstrated that a major improvement can be achieved in terms of temperature dependence. However, there are other design parameters, which can possibly influence the temperature dependence of the SFS output spectrum, such as fiber length and type, pump power, pump polarization, etc. This could yield further improvement of the temperature stability of the SFS. In this paper, we demonstrated that even with an already designed SFS setup, it is possible to reach a significant improvement in the temperature stability without any extra costs, added complexity, or power and bandwidth loss.

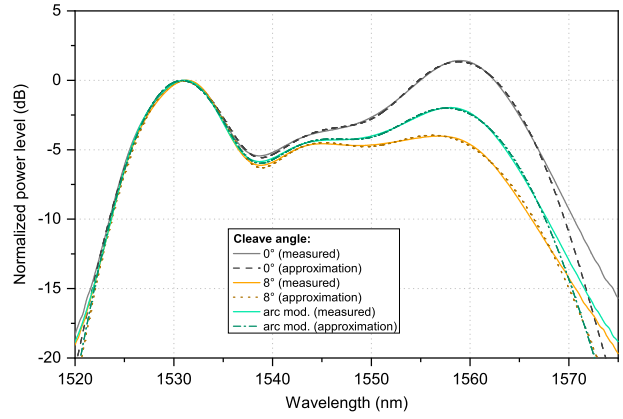

Fig. 10. Approximation of the SFS output spectra by a series of Gaussian functions for various fiber ends (20 °C).

V. Conclusion

We have demonstrated a fairly straightforward method for a significant improvement of the mean wavelength temperature stability $\partial\overline{\lambda}/\partial T$ of a backward-pump SFS by an adjustment of the reflection of the unpumped fiber end through an angled cleave and fusion arc. Introduction of a weak feedback (WF-DPB) to reflect a small portion of the forward ASE allows shaping of the SFS spectrum in a desired manner so that the ratio between the portion of the positive and negative contribution to the SFS mean wavelength temperature dependency can be controlled. This might be especially useful for compensation of these dependencies in other systems, such as FOGs, where the SFSs are typically utilized. Consequently, we were able to tune the slope K_T of the SFS temperature characteristics arbitrarily between -4.3 and 5.2 nm/°C. The standard deviation of $\overline{\lambda}(T)$ from the linear approximation was varying between 18 and 45 ppm in measurements over 140 °C range, which represents an additional instability of 0.32 ppm/°C in the worst case. Based on this method, we demonstrated an optimized WF-DPB having a slope K_T close to zero. Compared to the simple perpendicular cleave and the 8° cleave, we achieved a 32 and a 38-fold decrease in the slope K_T and a 5.7-fold and a 4.4-fold improvement in $\partial\overline{\lambda}/\partial T$ peak-peak mean wavelength variation. By avoiding any filtering components, high power efficiency of 22% as well as a spectral width of 38 nm was achieved. Due to the overall simplicity and cost-efficiency, the proposed method could be applicable in low and medium grade FOGs, where the total price is of a high importance.

References

[1] H. C. Lefèvre, "The fiber-optic gyroscope: Challenges to become the ultimate rotation-sensing technology", *Optical Fiber Technology*, vol. 19, no. 6, pp. 828–832, Dec. 2013.

[2] C. Ciminelli, F. Dell'Olio, C. E. Campanella, and M. N. Armenise, "Photonic technologies for angular velocity sensing", *Advances in Optics and Photonics*, vol. 2, no. 3, pp. 370–404, Jun. 2010.

[3] P. R. Morkel, "Erbium-doped fibre superfluorescent source for the fibre gyroscope", in *Optical Fiber Sensors: Proceedings of the 6th International Conference*, 1989, pp. 143–148.

[4] I. A. Andronova and G. B. Malykin, "Physical problems of fiber gyroscopy based on the Sagnac effect", *Physics-Uspekhi*, vol. 45, no. 8, pp. 793–817, Aug. 2002.

[5] P. F. Wysocki, M. J. F. Digonnet, B. Y. Kim, and H. J. Shaw, "Characteristics of erbium-doped superfluorescent fiber sources for interferometric sensor applications", *Journal of Lightwave Technology*, vol. 12, no. 3, pp. 550–567, Mar. 1994.

[6] A. S. Arabanian and R. Massudi, "Design and experimental realization of a highly efficient superfluorescent fiber source with flat C-band spectrum", *Optical Engineering*, vol. 54, no. 9, pp. 1–7, Sep. 2015.

[7] A. B. Petrov, R. Gumenyuk, M. S. Alimbekov, P. E. Zhelezov, N. E. Kikilich, A. S. Aleynik, I. K. Meshkovsky, K. M. Golant, Y. K. Chamorovskii, M. Odnoblyudov, and V. Filippov, "Broadband superluminescent erbium source with multiwave pumping", *Optics Communications*, vol. 413, pp. 304–309, 2018.

[8] X. Wang, "Stable L-band superfluorescent fiber source using one pump", *Optical Engineering*, vol. 48, no. 7, pp. 1–5, Jul. 2009.

[9] S. Hsu, T.-C. Liang, and Y.-K. Chen, "Optimum Configuration and Design of L-Band Erbium-Doped Superfluorescent Fiber Source", *Japanese Journal of Applied Physics*, vol. 41, no. Part 1, 6A, pp. 3724–3729, Jun. 2002.

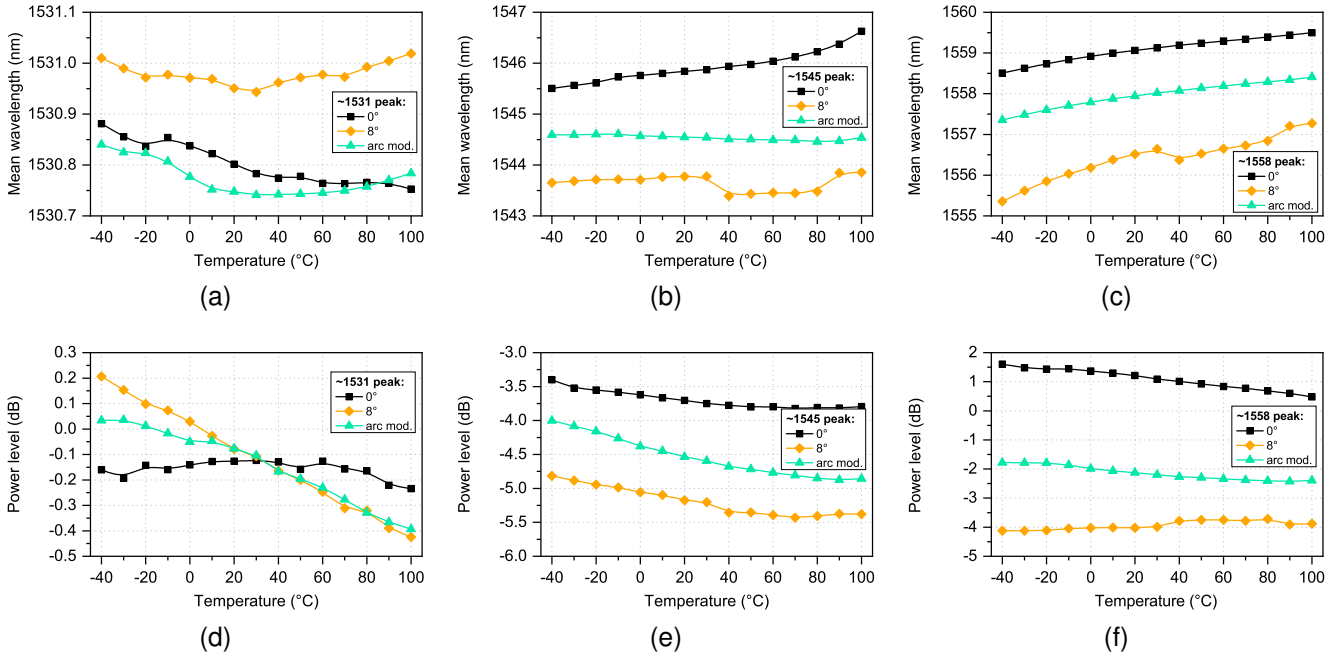

Fig. 11. Development of wavelength and power of the dominant peaks in the WF-DPB SFS output spectra with temperature for various fiber ends: (a, d) - 1531 nm peak, (b, e) - 1545 nm peak, (c, f) - 1558 nm peak, (Gaussian approximation).

[10] L. Zhu, W. He, Y. Zhang, F. Luo, and M. Dong, "A high flattening C + L band broadband source based on single pump and the same erbium-doped fiber", *Optik*, vol. 125, no. 17, pp. 4659–4662, Sep. 2014.

[11] D. Guillaumond and J.-P. Meunier, "Comparison of two flattening techniques on a double-pass erbium-doped superfluorescent fiber source for fiber-optic gyroscope", *IEEE Journal of Selected Topics in Quantum Electronics*, vol. 7, no. 1, pp. 17–21, Jan./Feb. 2001.

[12] C. Liu, X. Wu, J. Zhu, N. He, Z. Li, G. Zhang, L. Zhang, and S. Ruan, "Radiation-Resistant Er3+-Doped Superfluorescent Fiber Sources", *Sensors*, vol. 18, no. 7, p. 2236, Jul. 2018.

[13] A. A. Ponosova, I. S. Azanova, N. K. Mironov, M. V. Yashkov, K. E. Riumkin, O. L. Kel-, Y. O. Sharonova, and M. A. Melkumov, "Erbium-doped optical fibre with enhanced radiation resistance for superluminescent fibre sources", *Quantum Electronics*, vol. 49, no. 7, pp. 693–697, Jul. 2019.

[14] Y. Li, X. Wang, C.-X. Zhang, L.-J. Li, and Y.-F. Sun, "High stability double-pass backward Er-doped superfluorescent fiber source incorporating an Er-doped fiber filter", in *2014 International Conference on Multisensor Fusion and Information Integration for Intelligent Systems (MFI)*, 2014, pp. 1–4.

[15] H. J. Patrick, A. D. Kersey, W. K. Burns, and R. P. Moeller, "Erbium-doped superfluorescent fibre source with long period fibre grating wavelength stabilisation", *Electronics Letters*, vol. 33, no. 24, pp. 2061–2063, Nov. 1997.

[16] P. Ou, B. Cao, C. X. Zhang, Y. Li, and Y. H. Yang, "Er-doped superfluorescent fibre source with enhanced mean-wavelength stability using chirped fibre grating", *Electronics Letters*, vol. 44, no. 3, pp. 187–188, Jan. 2008.

[17] A. Wang, P. Ou, L. S. Feng, C. X. Zhang, X. M. Cui, H. D. Liu, and Z. Z. Gan, "High-Stability Er-Doped Superfluorescent Fiber Source Incorporating Photonic Bandgap Fiber", *IEEE Photonics Technology Letters*, vol. 21, no. 24, pp. 1843–1845, Oct. 2009.

[18] S.-C. Ruan, X. Wu, C.-X. Liu, and L. Zhang, "High-stability double-pass backward erbium-doped superfluorescent photonic crystal fiber source", in *23rd International Conference on Optical Fibre Sensors*, 2014, p. 9157AK.

[19] A. Wang, "High Stability Er-Doped Superfluorescent Fiber Source Improved by Incorporating Bandpass Filter", *IEEE Photonics Technology Letters*, vol. 23, no. 4, pp. 227–229, Feb. 2011.

[20] Y. Li, M. Jiang, C. X. Zhang, and H. J. Xu, "High Stability Er-Doped Superfluorescent Fiber Source Incorporating an Er-Doped Fiber Filter and a Faraday Rotator Mirror", *IEEE Photonics Technology Letters*, vol. 25, no. 8, pp. 731–733, Apr. 2013.

[21] X. Gong, B. Zhang, L. Xie, C. Zhang, X. Fan, L. Wei, W. Zhang, D. Jiang, W. Wang, K. T. Grattan, Y. Liao, and Z. -S. Zhao, "Research on temperature dependent mean wavelength stability of Erbium-doped fiber super fluorescent source for fiber optic gyroscopes", in *AOPC 2017: Fiber Optic Sensing and Optical Communications*, 2017, pp. 388–393.

[22] L. Yan, S. Yanfeng, W. Xu, and J. Man, "Er-doped superfluorescent fiber source with enhanced mean-wavelength stability incorporating a fiber filter", *Infrared and Laser Engineering*, vol. 44, no. 11, pp. 244–248, Jan. 2015.

[23] H. Wan, D. Zhang, and X. Sun, "Stabilization of a superfluorescent fiber source with high performance erbium doped fibers", *Optical Fiber Technology*, vol. 19, no. 3, pp. 264–268, Jun. 2013.

[24] J. Guo, T. Shen, G. Zhao, and Y. Yang, "Mean wavelength stable SFS with variable parameter control technology", in *Advanced Sensor Systems and Applications III*, 2007, pp. 409–414.

[25] H. C. Lefèvre, *The Fiber-Optic Gyroscope*, 2nd ed. London: Artech House, 2014.

[26] Y. Gronau and M. Tur, "Digital signal processing for an open-loop fiber-optic gyroscope", *Applied Optics*, vol. 34, no. 25, pp. 5849–5853, Sep. 1995.

[27] Q. Wang, C. Yang, X. Wang, and Z. Wang, "All-digital signal-processing open-loop fiber-optic gyroscope with enlarged dynamic range", *Optics Letters*, vol. 38, no. 24, pp. 5422–5425, Dec. 2013.

[28] T. P. Gaiffe, P. Simonpietri, J. Morisse, N. Cerre, E. M. Taufflieb,, and H. C. Lefevre, "Wavelength stabilization of an erbium-doped fiber source with a fiber Bragg grating for high-accuracy FOG", in *Fiber Optic Gyros: 20th Anniversary Conference*, 1996, pp. 375–380.

[29] Y. Yang, Y. -J. Rao, J. D. C. Jones, S. Yu, Z. Zheng, H. Naruse, R. I. Chen, W. Zhang, W. Jin, and X. Jiang, "Erbium-doped superfluorescent fiber source for fiber optic gyroscope", in *Advanced Sensor Systems and Applications*, 2002, pp. 111–114.

[30] D. G. Falquier, M. J. F. Digonnet, and H. J. Shaw, "A polarization-stable Er-doped superfluorescent fiber source including a Faraday rotator mirror", *IEEE Photonics Technology Letters*, vol. 12, no. 11, pp. 1465–1467, Nov. 2000.

[31] D. C. Hall, W. K. Burns, and R. P. Moeller, "High-stability Er^{3+}-doped superfluorescent fiber sources", *Journal of Lightwave Technology*, vol. 13, no. 7, pp. 1452–1460, Jul. 1995.

[32] M. Skalský, Z. Havránek, and J. Fialka, "Efficient Modulation and Processing Method for Closed-Loop Fiber Optic Gyroscope with Piezo-electric Modulator", *Sensors*, vol. 19, no. 7, 1710, Apr. 2019.

[33] E. Zhang, L. Yang, B. Xue, Z. Gao, Y. Zhang, and S. S.-H. Yam, "High thermal-stability Er-doped superfluorescent fiber source with a vertical

cleaved fiber tail", *Optical Fiber Technology*, vol. 58, p. 102262, Sep. 2020.

[34] E. Zhang, "Compensation for the temperature dependency of fiber optic gyroscope scale factor via Er-doped superfluorescent fiber source", *Optical Engineering*, vol. 57, no. 08, pp. 1–5, Aug. 2018.

[35] K. Okamoto, "Nonlinear Optical Effects in Optical Fibers", in *Fundamentals of Optical Waveguides*, 2.nd ed., Burlington: Academic Press, 2006, pp. 209–259.

[36] C. R. Giles and E. Desurvire, "Modeling erbium-doped fiber amplifiers", *Journal of Lightwave Technology*, vol. 9, no. 2, pp. 271–283, Feb. 1991.

[37] G. F. Tafti, A. Zareanborji, A. Ghaznavi, and Q. Zhao, "Measurement of Active Optical Fibers", in *Handbook of Optical Fibers*, G. Xiao, Ed. Singapore: Springer, 2019, pp. 1139–1176.

[38] E. Desurvire, *Erbium-Doped Fiber Amplifiers: Principles and Applications*. Wiley, 2002.

[39] Fibercore, "The IsoGain^{TM} Range of Erbium Doped Fibers", IsoGain fibers datasheet, Jul. 2008.

[40] D. E. McCumber, "Theory of Phonon-Terminated Optical Masers", *Physical Review*, vol. 134, no. 2A, pp. A299–A306, Apr. 1964.

[41] S.-C. Tsai, C.-M. Lee, S. Hsu, and Y.-K. Chen, "Characteristic comparison of single-pumped L-band erbium-doped fiber amplified spontaneous emission sources", *Optical and Quantum Electronics*, vol. 34, no. 11, pp. 1111–1117, Nov. 2002.

[42] P. F. Wysocki, M. J. F. Digonnet, and B. Y. Kim, "Wavelength stability of a high-output, broadband, Er-doped superfluorescent fiber source pumped near 980 nm", *Optics Letters*, vol. 16, no. 12, pp. 961–963, Jun. 1991.

[43] M. J. F. Digonnet, E. Murphy-Chutorian, and D. G. Falquier, "Fundamental limitations of the McCumber relation applied to Er-doped silica and other amorphous-host lasers", *IEEE Journal of Quantum Electronics*, vol. 38, no. 12, pp. 1629–1637, Dec. 2002.

[44] R. M. Martin and R. S. Quimby, "Experimental evidence of the validity of the McCumber theory relating emission and absorption for rare-earth glasses", *Journal of the Optical Society of America B*, vol. 23, no. 9, pp. 1770–1775, Sep. 2006.